◆ Human Brain Mapping 30:1535–1547 (2009) ◆

Automated White-Matter Tractography Using a Probabilistic Diffusion Tensor Atlas: Application to Temporal Lobe Epilepsy

Donald J. Hagler Jr.,[1,2]* Mazyar E. Ahmadi,[1,2] Joshua Kuperman,[1,2] Dominic Holland,[1,3] Carrie R. McDonald,[1,4] Eric Halgren,[1,2,3,4] and Anders M. Dale[1,2,3]

[1]*Multimodal Imaging Laboratory, University of California-San Diego, La Jolla, San Diego, California*
[2]*Department of Radiology, University of California-San Diego, La Jolla, San Diego, California*
[3]*Department of Neurosciences, University of California-San Diego, La Jolla, San Diego, California*
[4]*Department of Psychiatry, University of California-San Diego, La Jolla, San Diego, California*

Abstract: Diffusion-weighted magnetic resonance imaging allows researchers and clinicians to identify individual white matter fiber tracts and map their trajectories. The reliability and interpretability of fiber-tracking procedures is improved when a priori anatomical information is used as a guide. We have developed an automated method for labeling white matter fiber tracts in individual subjects based on a probabilistic atlas of fiber tract locations and orientations. The probabilistic fiber atlas contains 23 fiber tracts and was constructed by manually identifying fiber tracts in 21 healthy controls and 21 patients with temporal lobe epilepsy (TLE). The manual tract identification method required ~40 h of manual editing by a trained image analyst using multiple regions of interest to select or exclude streamline fibers. Identification of fiber tracts with the atlas does not require human intervention, but nonetheless benefits from the a priori anatomical information that was used to manually identify the tracts included in the atlas. We applied this method to compare fractional anisotropy—thought to be a measure of white matter integrity—in individual fiber tracts between control subjects and patients with TLE. We found that the atlas-based and manual fiber selection methods produced a similar pattern of results. However, the between-group effect sizes using the atlas-derived fibers were generally as large or larger than those obtained with manually selected fiber tracks. *Hum Brain Mapp 30:1535–1547, 2009.* © 2008 Wiley-Liss, Inc.

Key words: diffusion; probabilistic-atlas; epilepsy; fiber tracts; white matter; DTI

Additional Supporting Information may be found in the online version of this article.

Conflict of interest: Eric Halgren has equity interest in CorTechs Labs, and also serves on its Board of Directors. Anders M. Dale is a founder and holds equity in CorTechs Labs, and also serves on the Scientific Advisory Board. The terms of this arrangement have been reviewed and approved by the University of California, San Diego, in accordance with its conflict of interest policies.

The content is solely the responsibility of the authors and does not necessarily represent the official views of the National Institute of Neurological Disorders and Stroke or the National Institute of Health.

Contract grant sponsor: National Institute of Neurological Disorders and Stroke; Contract grant number: K23NS056091; Contract grant sponsors: GE Healthcare, mBIRN; Contract grant number: NS18741 (NINDS).

*Correspondence to: Donald J. Hagler Jr, 9500 Gilman Drive, Mail code 0841, La Jolla, CA 92093. E-mail: dhagler@ucsd.edu

Received for publication 29 February 2008; Revised 15 April 2008; Accepted 12 May 2008

DOI: 10.1002/hbm.20619
Published online 31 July 2008 in Wiley InterScience (www.interscience.wiley.com).

INTRODUCTION

Diffusion imaging (DI) is a form of magnetic resonance imaging (MRI) that can be used to estimate the diffusion coefficient of water along multiple orientations. Oriented diffusion can be represented, to first order, by a tensor [Basser et al., 1994]. In white matter, water diffusion occurs primarily along axons; so, the primary orientation estimated from diffusion tensor (DT) calculations can be used to infer white matter fiber orientations. Fractional anisotropy (FA) is a measure derived from DT calculations that describes the degree to which diffusion coefficients along the three orthogonal principal axes are different from each other. FA ranges from 0 to 1, with a value of 1 indicating diffusion exclusively in a single direction, and a value of 0 indicating isotropic diffusion. Gray matter tends to have a low FA (e.g., <0.15), while the FA of white matter depends on the population of fibers in a given voxel. Decreases in FA relative to normal controls for clinical populations are often used as a measure of white matter integrity, for example in the study of epilepsy [Yogarajah and Duncan, 2007]. It should be noted, however, that a number of factors could potentially affect FA; for example, myelination, the fraction of free water, the presence or absence of crossing fibers, etc. As such, FA may not be directly or exclusively related to white matter integrity, but it is a convenient and widely used measure.

Studies examining such differences typically use voxel-wise statistical comparisons, manually defined regions of interest (ROIs), or ROIs defined via white matter tractography methods. Statistical maps for voxel-wise analyses must be corrected for multiple comparisons and may lack statistical power compared to ROI analyses. Both voxel-wise and template-based ROI analyses require intersubject registration, which is often done with affine transformations (e.g., Talairach registration). Affine transformations do not necessarily provide good correspondence across subjects in the specific white matter fibers contained in a given atlas space location; so, apparent differences in FA or other measures could result from differences in fiber location rather than intrinsic fiber properties. Fiber tract ROIs defined with tractography methods are created for individual subjects to encompass all or part of particular fiber tracts, and can be used for group analyses as well as in clinical settings such as presurgical planning [Berman et al., 2007].

White matter tractography is generally done in two different ways; either with a method known as "deterministic" tractography [Basser et al., 2000; Conturo et al., 1999; Mori et al., 1999; Parker et al., 2002; Poupon et al., 2000], or with a "probabilistic" tractography method [Behrens et al., 2003, 2007; Friman et al., 2006; Jones and Pierpaoli, 2005; Lazar and Alexander, 2005]. With deterministic tractography, seeds are placed in voxels with FA greater than some threshold—e.g., 0.15 to include only white matter voxels—and then grown in both directions along the dominant diffusion orientation into fiber tracks or streamlines. Here, we use the term "tracks" to refer to one or more of these streamline paths, in distinction to the anatomical tracts themselves. As a track is extended into a neighboring voxel, the dominant diffusion orientation in that voxel determines where to next extend the track. A track is terminated when it reaches a voxel with subthreshold FA, or when the turning angle exceeds some threshold (e.g., 50°). Manually drawn ROIs are used to select tracks that pass through one or more regions, as well as to exclude tracks that stray into undesired locations because of crossing fibers or measurement noise [Catani et al., 2002; Conturo et al., 1999; Mori et al., 2002; Stieltjes et al., 2001; Wakana et al., 2004]. It is necessary to use or develop an ROI selection strategy for each fiber tract of interest, guided by anatomical knowledge of the trajectory of known fiber tracts.

Probabilistic tractography methods probe the fiber orientation probability distributions at each voxel, assessing the likelihood of a fiber following a particular path, given the diffusion data. Advantages of this method over the deterministic method include the ability to explicitly represent uncertainty in the data [Behrens et al., 2003]. In addition, probabilistic tractography methods can more reliably reconstruct crossing fibers [Behrens et al., 2007; Berman et al., 2008]. A disadvantage, however, is that it requires thousands of iterations, and is thus computationally intensive. Like the deterministic tracking method, prior knowledge of the anatomy of fiber tracts is important for distinguishing between fiber tracts of interest and streamline tracks that follow improbable routes or suggest nonexistent connections between brain areas.

An alternative approach is to view the identification of fiber tracts as a segmentation problem, analogous to that of segmenting subcortical structures from T_1-weighted MR images. In that case, voxels belonging to particular subcortical structures can be identified using a combination of image intensity and prior information—in the form of a probabilistic atlas—about the likelihood of a particular label given the location in atlas space [Fischl et al., 2002]. In this study, we describe an extension of this segmentation approach to the labeling of white matter fiber tracts in individual subjects by using diffusion-weighted images, T_1-weighted images, and a probabilistic atlas of fiber tract locations and orientations. The fiber atlas contains 23 fiber tracts, 20 of which are made up of 10 left-right hemisphere pairs. Since this method requires no human intervention, other than in the construction of the atlas, interoperator variability is eliminated. Our results from applying this method to a cohort of patients with temporal lobe epilepsy (TLE) and age-matched healthy controls suggest that the group effect sizes are comparable or greater than using manual procedures. Thus, it has the potential to be of great utility in both research and clinical settings.

METHODS

Human Subjects

All participants provided written consent prior to enrollment in the study, which was approved by the Institu-

tional Review Board. Twenty-one healthy control subjects (ages 21–52, mean 33, std 10.2 years) were recruited through open advertisement. This control group consisted of 11 females and 10 males with no known history of neurological disorder, loss of consciousness, or serious medical or psychiatric condition. Twenty-one patients with TLE were also enrolled in the study (ages 21–54, mean 37.3, std 10.0 years). All patients were recruited from the University of California, San Diego, Epilepsy Center, and diagnosed by a board-certified neurologist with expertise in epileptology. The patient and control groups were age- and gender-matched, with no significant difference in mean age. Handedness in all participants was assessed with the Edinburgh Handedness Inventory [Oldfield, 1971]. Two control subjects and two patients with left TLE were left-handed. One patient with left TLE was excluded after it was discovered that incorrect scan parameters were used during collection of the diffusion data (b = 2,000 instead of b = 1,000).

Patients were classified as left or right TLE according to video-EEG telemetry, seizure semiology, and neuroimaging results. Subjects with either an epileptic focus or radiological evidence of pathology outside the temporal regions were excluded. In all 21 patients with TLE, the diagnosis was based on the presence of ictal and interictal temporal-lobe epileptiform activity as monitored by video-EEG telemetry. In the majority of patients, scalp recordings were supplemented with sphenoidal electrodes. When necessary, patients underwent monitoring with five-contact foramen ovale electrodes to confirm mesial temporal onset. According to these criteria, eleven patients were diagnosed with unilateral right TLE and ten with unilateral left TLE. Diagnoses were supported in 16 of 21 patients by the presence of hippocampal atrophy and increased signal on T_2-weighted images, consistent with mesial temporal sclerosis (MTS). In no case was there evidence of dual-pathology on MRI. The remaining five patients showed no evidence of MTS based on visual inspection by a neuroradiologist with expertise in epilepsy. The imaging protocol was identical for all participants, and all patients were seizure-free for a minimum of 24 h prior to the MRI scan to avoid the possible effects of acute postictal changes on diffusion parameters.

Image Acquisition

MRI was performed at the UCSD Radiology Imaging Laboratory on a General Electric 1.5 T EXCITE HD scanner with an eight-channel phased-array head coil. Image acquisitions included a conventional three-plane localizer, GE calibration scan, two T_1-weighted 3D structural scans (TE = 3.8 ms, TR = 10.7 ms, TI = 1 s, flip angle = 8°, bandwidth = 15.63 kHz, FOV = 25.6 cm, matrix = 192 × 192, slice thickness = 1.0 mm), and five diffusion-weighted (DW) sequences. Diffusion data were acquired using single-shot echo-planar imaging with isotropic 2.5 mm voxels (matrix size = 96 × 96, FOV = 24 cm, 47 axial slices, slice thickness = 2.5 mm), covering the entire cerebrum and brainstem without gaps. Three volume series were acquired with 51 diffusion gradient directions using b-values of 600 s/mm^2 (TE/TR 68.4/10,900), 800 s/mm^2 (TE/TR 72.3/11,700), and 1,000 (TE/TR 75.6/12,300) s/mm^2, each with an additional b = 0 volume. For use in nonlinear B_0 distortion correction, two additional series were acquired with opposite phase encoding polarity.

Image Processing

Image files in DICOM format were transferred to a Linux workstation for processing with a customized, automated, processing stream written in MATLAB and C++. The two T_1-weighted images were rigid body registered to each other and reoriented into a common space, roughly similar to alignment based on the anterior/posterior commissure line. Images were corrected for nonlinear warping caused by nonuniform fields created by the gradient coils [Jovicich et al., 2006]. Image intensities were corrected for spatial sensitivity inhomogeneities in the eight-channel head coil by normalizing with the ratio of a body coil scan to a head coil scan (calculated from the GE PURE calibration scan).

Five preprocessing steps were performed on the diffusion-weighted images: (1) Head motion between scans was removed by rigid body registration between the b = 0 images of each DW scan; (2) Within-scan motion was removed using a novel method involving the calculation of DTs (see below for details of DT calculations), synthesis of DW volumes from those tensors, and rigid body registration between each data volume and its corresponding synthesized volume. This method avoids the simplifying assumption that the intensity correlation between DW volumes will be maximal when they are properly aligned, which is incorrect, since image intensity will vary between diffusion orientations; (3) Image distortion in the DW volumes caused by eddy currents was minimized by nonlinear optimization with four free parameters for each DW volume (translation along the phase-encode direction and scaling along phase-encode direction as a linear function of x, y, or z); (4) Image distortion caused by magnetic susceptibility artifacts was minimized with a nonlinear B_0-unwarping method (D. Holland, D.J. Hagler Jr., and A.M. Dale, in preparation) using paired images with opposite phase-encode polarities [Chang and Fitzpatrick, 1992; Morgan et al., 2004; Reinsberg et al., 2005]. This method corrects for nearly all image distortion caused by magnetic susceptibility artifacts and enables highly accurate registration with the T_1-weighted images; (5) Images were resampled using linear interpolation to have 1.875 mm isotropic voxels (63 axial slices). Even though images were acquired with isotropic resolution of 2.5 mm, the images were automatically zero-padded in k-space from 96 × 96 to 128 × 128, and reconstructed with 1.875 × 1.875 × 2.5 mm^3 voxels.

Correction for Differences in Intensity Scaling

Because the three different b-value diffusion scans were collected with three different echo times, the MR signal

TABLE I. Brief descriptions of fiber tracts included in atlas

Fiber name	Description
Corpus callosum	Major bundle of interhemispheric connections
Forceps major	Posterior, occipital portion of corpus callosum
Forceps minor	Anterior, frontal portion of corpus callosum
Cingulum (cing)	Cingulate portion of cingulum: connects cingulate gyrus and entorhinal cortex
Cingulum (hipp)	Parahippocampal portion of cingulum
Fornix	Connects hippocampus and mammilary nuclei of hypothalamus
IFOF	Inferior frontal occipital fasciculus: connects occipital and frontal lobes
ILF	Inferior longitudinal fasciculus: connects occipital and temporal lobes
Pyramidal	Pyramidal or corticospinal tract: connects motor cortex and spinal cord
SLF	Superior longitudinal fasciculus: connects temporal and parietal lobes with frontal lobe
tSLF	Portion of SLF that ascends from temporal lobe and connects to frontal lobe (arcuate fasciculus)
Anterior thalamic	Anterior thalamic radiations: connects thalamus with frontal lobe
Uncinate	Connects inferior frontal and anterior temporal lobes

variations depend not only on diffusion properties, but also on T_2 time constants. The scanner used automatically scales the data such that these differences in signal intensity are reduced, but not eliminated. To correct for residual differences in intensity scaling, additional scaling factors were applied to each of the three diffusion scans. The scaling factors were obtained by calculating the mean signal of the $b = 0$ images. To exclude nonbrain and CSF, only voxels within the 75th and 95th percentiles of signal intensity were included in the mean calculation.

Diffusion Tensor Calculations

DTs were calculated using linear inversion after taking the log of the data, thus performing a monoexponential fit across the three b-values, constrained by the three $b = 0$ volumes and 153 DW volumes (51 independent directions). DTs were also calculated for individual scans with single b-values. DTs derived from the three b-values were used for manually assisted fiber-tracking, whereas DTs derived from the $b = 1{,}000$ images alone were used for ROI FA measurements. To account for the rotations required for correcting head motion (preprocessing steps 1 and 2 described above), the 51 diffusion gradient vectors used by the diffusion pulse sequence were rotated with that component of the motion correction transformation matrices. The tensor matrices were diagonalized using singular value decomposition, obtaining three eigenvectors and three corresponding eigenvalues. The FA ratio was calculated from the eigenvalues according to Eq. (1):

$$\mathrm{FA} = \sqrt{\frac{3}{2}\frac{(\lambda_1 - \bar{\lambda})^2 + (\lambda_2 - \bar{\lambda})^2 + (\lambda_3 - \bar{\lambda})^2}{\lambda_1^2 + \lambda_2^2 + \lambda_3^2}} \qquad (1)$$

where λ_i is the ith eigenvalue and $\bar{\lambda}$ is the mean of the eigenvalues.

Manually Assisted Fiber-Tracking Using DTI Studio

DTI Studio (Laboratory of Brain Anatomical MRI, Johns Hopkins Medical Institute) is freely available software for deterministic fiber-tracking that was used to generate streamline tracks for 23 fiber tracts. Brief descriptions of the fiber tracts included in the study can be found in Table I. Two of the fibers, the forceps major and forceps minor, are subsets of the corpus callosum. The remaining 20 fibers comprise 10 bilateral fiber pairs. The right and left temporal superior longitudinal fasciculi (tSLF) are subsets of the right and left SLF. The cingulum bundles are represented in two separate, cingulate and hippocampal portions. This separation is done primarily because of the crossing fibers between the two portions of the tract making it difficult or impossible to generate streamlines tracing the entire cingulum with the deterministic tracking algorithm.

FA and first eigenvector (V0) volumes were exported to DTI Studio to generate fiber tracks for use as a training set for the fiber atlas. DTI Studio uses the "fiber assignment continuous tracking" (FACT) algorithm to connect voxels with similar diffusion orientations into fiber tracks [Mori et al., 1999]. Seed points were placed at the center of all voxels with FA > 0.15 (essentially excluding nonwhite matter), and fiber tracks were extended until reaching a voxel below that FA threshold or when the fiber track turned by more than a particular angle threshold, in this case 50 degrees [Conturo et al., 1999]. It was particularly difficult to obtain complete fornix tracks using those settings; so, for the fornix, fiber-tracking was done with an angle threshold of 40 degrees and FA threshold of 0.07. All fibers tracks were then subsequently thresholded to exclude voxels with FA < 0.15.

Each fiber tract was identified using multiple ROIs to select a population of streamlines that followed the paths known from anatomy [Wakana et al., 2004]. Additional ROIs were used to either eliminate or truncate stray fibers that did not conform to a priori knowledge about the particular fiber tract. These manually assisted fiber-tracking procedures have been previously shown to be quite reliable, even for operators without previous fiber-tracking experience [Wakana et al., 2007]. In the current study, the author who performed the manual fiber-tracking (M.E.A.) spent several months practicing and refining strategies for

consistently and efficiently tracking each fiber tract. All of the manually assisted fibers tracks included in the present study were generated at the end of this process, in a period of less than a month. The tracking procedure took ~2–3 min per fiber tract. Thus, the manual work involved in generating the atlas training set for the 42 subjects and 23 fiber tracts took ~40 h.

The tracking strategies that performed well for most subjects did not necessarily result in satisfactory tracks for all subjects. The presence of crossing fibers is the primary explanation for why a particular tracking strategy may not perform well. For example, all of the streamlines modeling a particular fiber tract may turn and follow a different fiber tract, such that no streamlines actually follow the path of the tract of interest from start to finish. It may have been possible to develop customized tracking strategies for each tract and each subject, but instead of doing that, standardized tracking strategies were used, and tracks were included only when they mapped the full trajectory of the fiber tract of interest. The number of subjects included in the atlas for each fiber is summarized in Supporting Information Table I.

Three-dimensional maps of streamline fiber counts, which we will refer to as fiber density maps, were used to summarize the information obtained from fiber-tracking with DTI Studio. Although the number of streamlines in a particular voxel probably does not linearly relate to the density of axons per unit volume, it does indicate the relative likelihood that the voxel truly belongs in the fiber tract of interest. These fiber density maps were used to calculate weighted ROI averages of FA, and provided the location information for the fiber atlas (see below).

Intramodality Image Registration

Accurate registration between T_2-weighted (e.g., $b = 0$ images of DW scans) and T_1-weighted images is a challenge and requires specialized registration methods. For initial, rough alignment, the T_2-weighted images were first rigid-body-registered (using intensity correlation) to an average of 10 subjects' T_2-weighted images that had been previously registered to corresponding T_1-weighted images resampled to atlas space. Fine registration between the T_2- and T_1-weighted images was then done using the joint probability density function (JPDF) method [Leventon and Grimson, 1998]. The JPDF, a 2-D histogram of intensity values in the T_1- and T_2-weighted images, was generated for each of the 10 previously registered T_2-weighted images and then averaged across subjects. Those 10 T_2-weighted images were themselves aligned to their corresponding T_1-weighted images by using a JPDF calculated from a single subject's manually aligned T_2-weighted image. Subjects with poor alignment based on this initial JPDF were not included in the average JPDF. The average JPDF was able to provide excellent registration (each was visually inspected for registration accuracy) for all subjects.

Construction of Fiber Location and Orientation Atlas

The T_1-weighted volume for each subject was nonlinearly morphed into alignment with a T_1-weighted atlas volume using the method of discrete cosine transforms with 125 degrees of freedom [Friston et al., 1995]. DW images were rigid-body-registered to the T_1-weighted images as described above, and the resulting transformation matrix was used to resample the fiber density volumes generated using DTI Studio into the T_1-space; they were then nonlinearly warped into the T_1-weighted atlas space using the previously calculated nonlinear transformation for the T_1-weighted volume.

These coregistered fiber density maps were averaged across subjects. The average fiber density values were then normalized to the maximum average value for each fiber tract. These normalized, average fiber density maps show the relative probability that a fiber tract occupies a given location. The first eigenvectors for each subject were rotated into alignment with the atlas using the registration to T_1 and the rigid-body component of the registration to atlas, and then resampled into atlas space. The tensor outer product of these rotated first eigenvectors was calculated, and then for each fiber, smoothed using a specialized tensor smoothing method (described below). We then calculated a cross-subject average tensor containing information about the range of possible diffusion orientations at each location in atlas space.

Voxels included in the fiber masks sometimes had first eigenvectors that conflicted with the general trajectory of the fiber bundle and their neighboring voxels. This was apparently caused either by streamlines straying into neighboring fiber tracts or by crossing fibers. The tensor smoothing method was designed so that orientation information used in the atlas reflected the overall trajectory of the fiber bundle and excluded conflicting orientations calculated from DT fitting within single subject fiber masks (see Fig. 4). The smoothed tensor for a voxel was the weighted average of values within a three-voxel-radius neighborhood. The weighting used was a dominance ratio (DR) calculated from DT eigenvalues that compares the first eigenvalue to the second:

$$\mathrm{DR} = \frac{\mathrm{abs}(\lambda_1 - \lambda_2)}{\lambda_1} \tag{2}$$

where λ_i is the ith eigenvalue. DR is largest for voxels with diffusion along a single direction.

Automated, Atlas-Based Tract Identification

The atlas, containing probabilistic information about the locations and orientations of each fiber tract, was used to estimate the *a posteriori* probability that a given voxel belongs to a particular fiber tract. The fiber probability distribution for a single subject is described by Eq. (3):

$$P(f|\ v) \propto P(v|f) \times P(f) \tag{3}$$

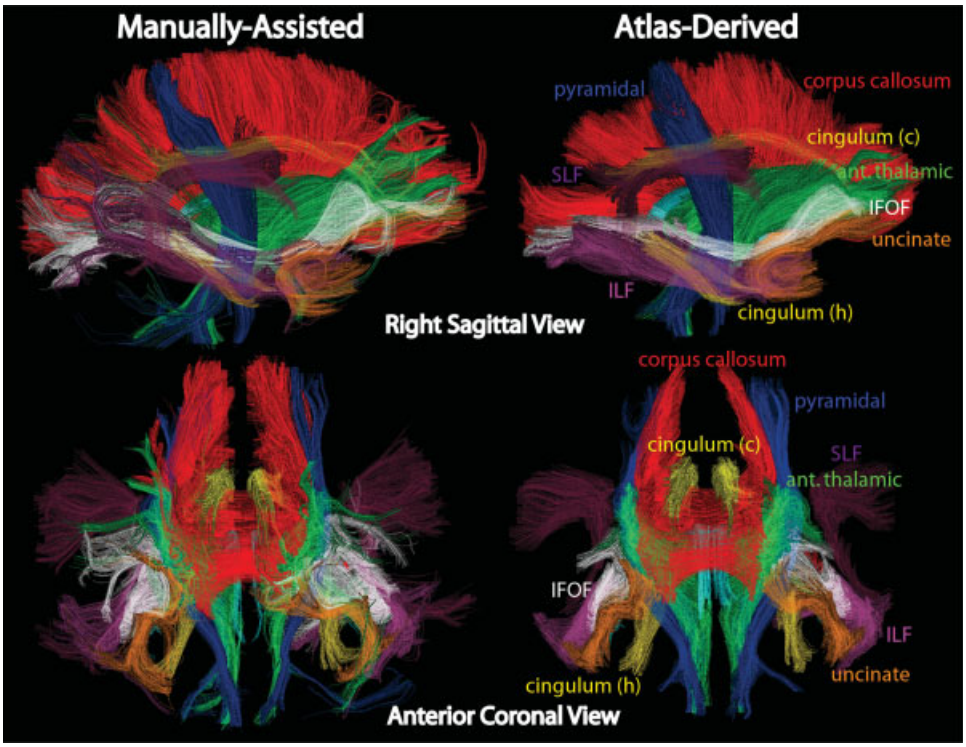

Figure 1.

Comparison of manually selected and atlas-derived fiber tracks. Tracks for all fibers excluding forceps major and minor (subsets of corpus callosum) and tSLF (subset of SLF) are shown. Atlas-derived fiber tracks were generated using FACT algorithm within fiber ROIs [relative fiber probability (RFP) $>$ 0.07, FA $>$ 0.15]. Fiber tracks for one representative control subject are presented. [Color figure can be viewed in the online issue, which is available at www.interscience. wiley.com.]

where $P(f|v)$ is the probability of a voxel belonging to a given fiber tract given the first eigenvector v derived from DT calculations. $P(f)$ is the fiber probability given location alone, and is equal to the normalized, average fiber density described above after resampling from atlas space to single-subject-space. $P(v|f)$ is the fiber probability given the DT first eigenvector and was estimated using the atlas average of DTs (rotated and warped into single subject space) according to Eq. (4):

$$P(v|f) = \frac{v'\overline{T}v}{\bar{v}'\overline{T}\bar{v}} \quad (4)$$

where $\overline{T}$ is the atlas tensor generated as described above, v is the first eigenvector of a single subject's DT matrix, v' is its transpose, and $\bar{v}$ is the first eigenvector of $\overline{T}$. In this case, the denominator is equal to the first eigenvalue of $\overline{T}$.

Maps of the a posteriori probability calculated with Eq. (3), which we will refer to as atlas-derived fiber ROIs, were used to calculate weighted averages of FA [Hua et al., 2008]. Voxels with FA less than 0.15 were excluded to facilitate comparisons with the manually selected fiber tracks, which were generated using the same threshold. For comparison, ROI FA measures were also calculated without this FA threshold (see "Results" section). To visually compare atlas-derived fiber masks with manually selected fiber tracks, we generated streamline tracks within the atlas-derived fiber masks using DTI Studio's fiber assignment by continuous tracking (FACT) algorithm [Mori et al., 1999]. The atlas-derived fiber masks were generated from the fiber probability maps by applying a probability threshold. We selected a threshold by testing a range of thresholds, calculating the volume of suprathreshold voxels, and choosing the threshold that provided the smallest difference in fiber volumes between manually selected and atlas-derived fiber masks across all subjects and fibers.

RESULTS

We have developed a method for automatically labeling white matter fiber tracts that uses information from single subject diffusion data and a probabilistic fiber atlas (see "Methods" section). The atlas consists of averaged information about the locations and local orientations of the chosen fiber tracts. Fiber ROIs were derived from the atlas

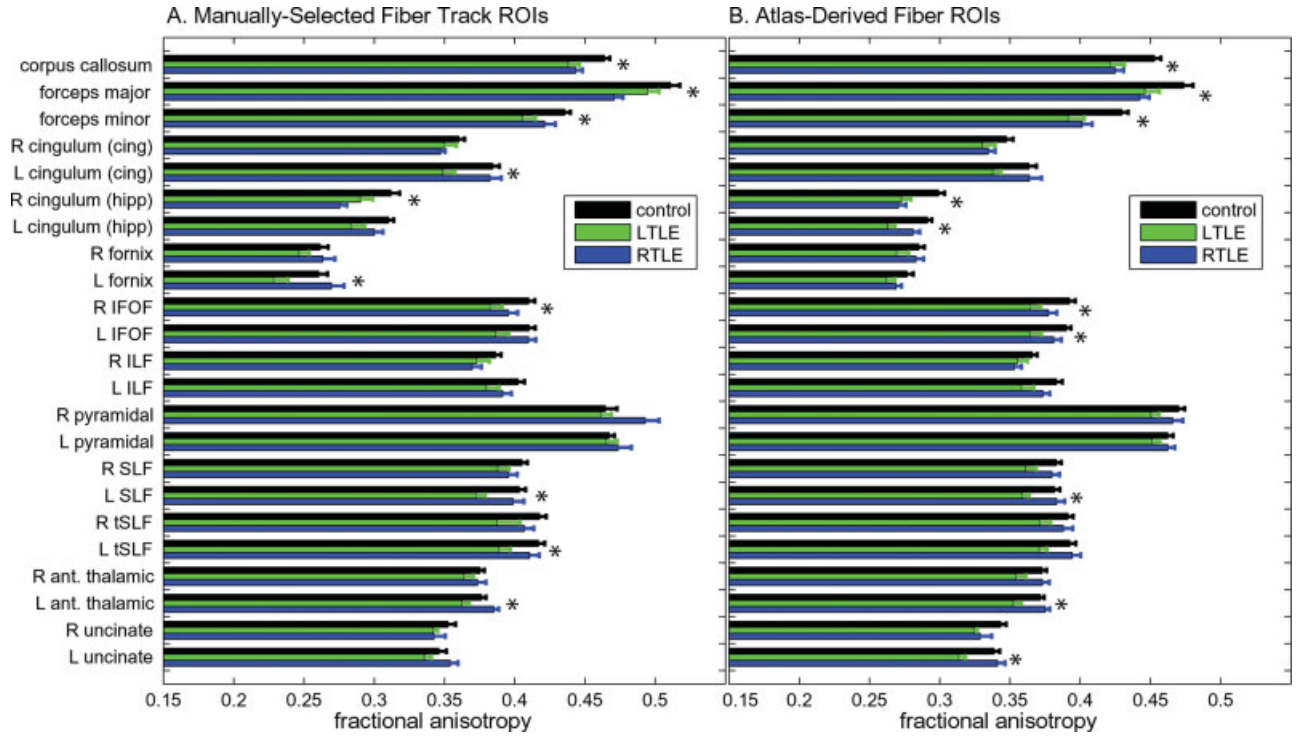

Figure 2.

Weighted mean of fractional anisotropy of white matter in control subjects and patients with right and left TLE for (**A**) manually-selected fiber tracks and (**B**) atlas-derived fiber ROIs. Error bars represent SEM. Voxels with FA less than 0.15 were excluded. Fiber tracts with significant ($P < 0.01$) group effects (ANOVA) are indicated with asterisks (*). See Table II. [Color figure can be viewed in the online issue, which is available at www.interscience.wiley.com.]

for single subjects using both T_1-weighted images and orientation estimates from DT calculations. The T_1-weighted images were used to map the brain into a common space, and DT orientation estimates were compared to the atlas to obtain a relative probability that a voxel belongs to a particular fiber given the similarity of diffusion orientations (see "Methods" section). Figure 1 compares fiber tracks obtained through manually assisted and atlas-based methods in an individual control subject. Fiber tracks for additional subjects are shown in Supporting Information Figures 1 and 2.

Average FA values were calculated for both manually selected fiber tracks and atlas-derived fiber ROIs (see Fig. 2). It should be noted that the tractography method used by DTI Studio excludes voxels from fiber tracks when the FA is lower than a threshold value such as 0.15. As described in "Methods" section, this same FA threshold was applied to the atlas-derived fiber ROIs. Average FA values were also calculated for atlas-derived fiber ROIs without FA thresholds (Supp. Info. Fig. 3). The average FA values—calculated separately for control subjects and for patients with left and right TLE—for manually selected fiber tracks and atlas-derived fiber ROIs were highly correlated ($R^2 = 0.98$ with FA threshold, $R^2 = 0.97$ without threshold). Average FA values for atlas-derived fiber values were slightly lower than those for manually selected fiber tracks (normalized difference averaged across fibers: 3.1 ± 0.8% SEM; t test $P < 10^{-3}$). When the FA threshold was not applied to the atlas-derived fiber ROIs, the average FA measures were further reduced relative to manually selected fiber tracks (normalized difference averaged across fibers: 13.1 ± 1.0% SEM; t test $P < 10^{-11}$). The average coefficient of variation (standard deviation/mean) across all fiber tracts was slightly lower for atlas-derived fiber ROIs (5.9 ± 0.2% SEM) versus manually selected fiber tracks (6.6 ± 0.4% SEM) ($P < 0.05$, paired t test).

Manually selected fiber tracks revealed differences between control and patients with right and left TLE (one-way ANOVA across the three groups for each fiber tract), and a similar pattern of results was observed with the atlas-derived fiber ROIs (Fig. 2, Table II, Supp. Info. Tables II–IV). Overall, there was a trend that patients with TLE, particularly those with a left hemisphere epileptic focus, exhibited widespread, bilateral decreases in FA across fiber tracts relative to controls. Inspection of Table II reveals that parametric tests of group differences (i.e., ANOVAs) were generally associated with higher levels of statistical significance (i.e., lower P values) for atlas-derived fiber

TABLE II. ANOVA *F*-statistics from manually selected and atlas-derived fibers for control subjects, patients with left TLE, and patients with right TLE

	Manual		Atlas		Atlas (no threshold)	
Fiber name	*F*-stat	*P*	*F*-stat	*P*	*F*-stat	*P*
Corpus callosum	**7.57**	**0.0017**	**8.56**	**0.0009**	**7.53**	**0.0018**
Forceps major	**8.15**	**0.0011**	**5.49**	**0.0081**	4.20	0.0225
Forceps minor	**5.86**	**0.0060**	**9.38**	**0.0005**	**7.91**	**0.0013**
R cingulum (cing)	1.90	0.1638	2.45	0.0999	2.03	0.1458
L cingulum (cing)	**7.44**	**0.0019**	3.95	0.0277	1.83	0.1742
R cingulum (hipp)	**7.75**	**0.0015**	**10.35**	**0.0003**	**10.68**	**0.0002**
L cingulum (hipp)	5.17	0.0104	**11.50**	**0.0001**	**11.52**	**0.0001**
R fornix	1.38	0.2659	2.06	0.1413	1.28	0.2908
L fornix	**5.32**	**0.0093**	2.17	0.1282	1.72	0.1928
R IFOF	**5.24**	**0.0098**	**6.49**	**0.0038**	**5.69**	**0.0069**
L IFOF	4.25	0.0216	**6.36**	**0.0042**	**5.94**	**0.0057**
R ILF	2.70	0.0802	2.29	0.1155	2.19	0.1262
L ILF	3.36	0.0455	4.69	0.0151	**6.03**	**0.0053**
R pyramidal	3.04	0.0595	2.96	0.0641	2.33	0.1108
L pyramidal	0.37	0.6910	1.57	0.2212	2.31	0.1130
R SLF	2.42	0.1025	4.82	0.0136	4.77	0.0142
L SLF	**6.58**	**0.0036**	**6.73**	**0.0031**	**5.35**	**0.0090**
R tSLF	3.38	0.0476	3.42	0.0430	4.17	0.0230
L tSLF	**5.24**	**0.0099**	4.89	0.0129	4.61	0.0161
R anterior thalamic	1.38	0.2649	4.33	0.0203	5.00	0.0118
L anterior thalamic	**6.18**	**0.0047**	**8.41**	**0.0009**	**8.33**	**0.0010**
R uncinate	1.02	0.3699	4.10	0.0245	3.20	0.0521
L uncinate	1.81	0.1779	**7.62**	**0.0016**	**7.27**	**0.0021**

For each tract, a separate, one-way ANOVA was calculated across groups.Bold typeface indicates $P < 0.01$.

ROIs compared to manually selected fiber tracks. To identify tracts with significant group effects, we chose a threshold of $P < 0.01$, which we estimated results in a false discovery rate (FDR) of less than 0.03 [Genovese et al., 2002]. That is, out of 100 positive results, less than three are expected to be false.

Utility of Orientation Information in Tract Identification

The atlas includes both location and orientation information for individual fiber tracts. To obtain fiber probability maps based on location alone, T_1-weighted MR images are sufficient for nonlinear registration with the atlas. The inclusion of DI data refines the maps and individualizes them for each subject. This refinement is particularly important in resolving ambiguity between proximal fibers with different orientations (see Fig. 3). Because two fiber tracts such as the corpus callosum and cingulum are close to each other, the location probability maps overlap. The local orientations of these fiber tracts are roughly perpendicular to each other, which makes it possible to distinguish the two fiber tracts based on the fiber orientation atlas.

It should be noted that the orientation information used in the atlas is first filtered by local neighborhood smoothing in individual subjects (see Fig. 4). When two or more fibers occupy a single voxel, the estimated orientation may be dominated more by one fiber than the other, or may be more or less random. Furthermore, streamline fiber tracks may sometimes stray slightly into neighboring tracts. With orientation smoothing, the orientations are forced to be consistent with the overall trajectory of the fiber tract of interest, making it possible to distinguish between neighboring fiber tracts like the corpus callosum and cingulum (see Fig. 3).

DISCUSSION

The probabilistic atlas-based method presented here enables fully automated identification of several major fiber tracts in individual subjects. We applied this method to the study of TLE, comparing control subjects to patients with left and right TLE. Other potential applications include studies of different patient populations, as well as studies of normal development and aging. An advantage of our method over commonly used manually assisted fiber-tracking methods is that it requires no human intervention. Because of this, it makes large-scale studies of white matter fiber tracts more practical and efficient and removes any concern about potential inter-operator variability. This method of identifying white matter fiber tracts is similar in principle to previous methods for automated segmentation of subcortical structures using T_1-weighted images [Fischl et al., 2002]. One important difference is that the white matter fiber tract assignments are not mutually exclusive like the subcortical structure labels; that is, two or more fiber tracts may occupy the same voxel. We constructed our fiber atlas in T_1-weighted space such that the fiber ROIs can be created in the same space as subcortical and cortical ROIs. Together, these methods provide a means for efficiently obtaining ROI measures of tissue properties such as FA, ADC, T_1, etc. for both subcortical structures and white matter fibers tracts.

Effect sizes for between-group comparisons – and thus statistical power – were, in general, as large or larger for atlas-derived fiber ROIs compared to manually selected fiber tracks. Because of the strong location and direction priors introduced by the probabilistic atlas, this method is less susceptible to noise in the DI data than the more commonly used streamlining methods [Basser et al., 2000; Conturo et al., 1999; Mori et al., 1999; Parker et al., 2002; Poupon et al., 2000]. Stray tracks following routes that do not conform to the known anatomy of particular tracts may be produced with fiber-tracking, but will contribute minimally to the atlas-derived fiber ROIs. Regions with low FA (e.g. lesions) or crossing fibers will typically interfere with fiber-tracking, but will not prevent the probabilistic atlas method from identifying those other parts of the fiber tract that are consistent with the atlas. The extensive manual editing involved in generating the fiber tracks was necessary to achieve a probabilistic atlas that accurately reflects white matter anatomy, but no manual editing is required when applying the atlas to new data. Subject populations other than healthy adults and patients with

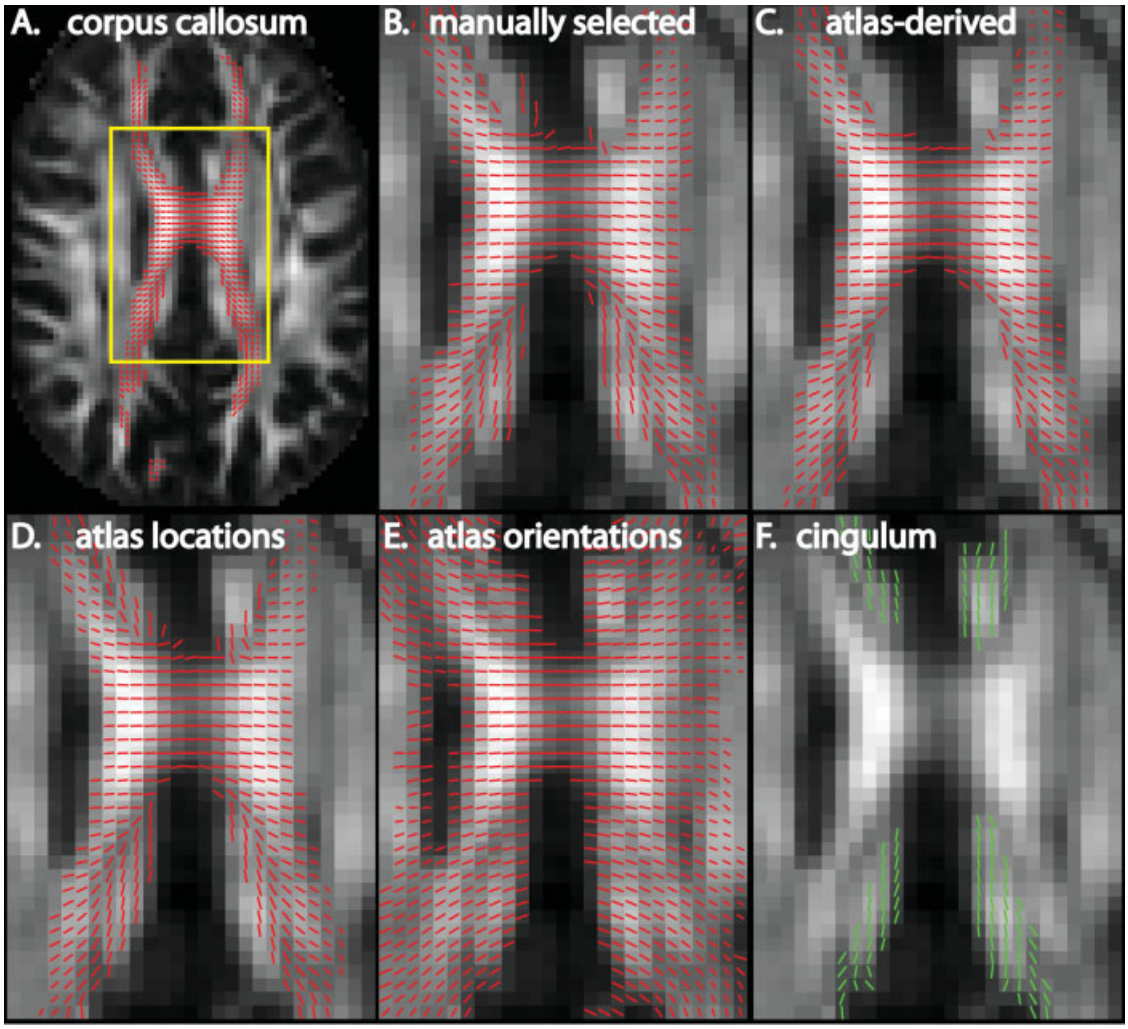

Figure 3.

Refinement of atlas-derived fiber ROIs with orientation information. Diffusion orientations of voxels within fiber ROIs are plotted as line segments, overlayed on an axial slice of the FA volume for a control subject. (**A**) Atlas-derived fiber ROI (RFP $>$ 0.07, FA $>$ 0.15) for corpus callosum, shown in the full slice, with yellow rectangle marking the region shown in B–F. (**B**) Manually selected fiber track ROI (voxels with at least one streamline). (**C**) Atlas-derived fiber ROI (same as in A). (**D**) Atlas-derived fiber ROI, using location information only (RFP $>$ 0.10, FA $>$ 0.15). (**E**) Corpus callosum fiber orientations from atlas (not individual subject data like A–D and F) for all voxels with RFP $>$ 0. (**F**) Atlas-derived fiber ROIs for left and right cingulum bundles. [Color figure can be viewed in the online issue, which is available at www.interscience.wiley.com.]

TLE may exhibit somewhat different white matter tract trajectories, so application to other populations, such as children, may require adding to the atlas manually selected fiber tracks from a sample of that target population before successful application of this method.

Comparison of Manually Selected Fiber Tracks and Atlas-Derived Fiber ROIs

There is a striking, qualitative difference between manually selected fiber tracks and those selected using atlas-derived fiber masks (see Fig. 1). The prior information supplied by the atlas eliminates the stray fibers that are difficult to avoid with manually selected fiber tracks, making extensive and time-consuming manual editing unnecessary. Despite the qualitative differences, the average measures of FA for atlas-derived and manually selected fibers were highly correlated. Between group comparisons of control subjects and patients with TLE were also similar for both manually selected fiber tracks and atlas-derived fiber ROIs. Differences between the two sets of results may be attributable to deviations from true anatomy in the manually selected fiber tracks. The variability of FA measurements, as quantified by the coefficient of variation, was

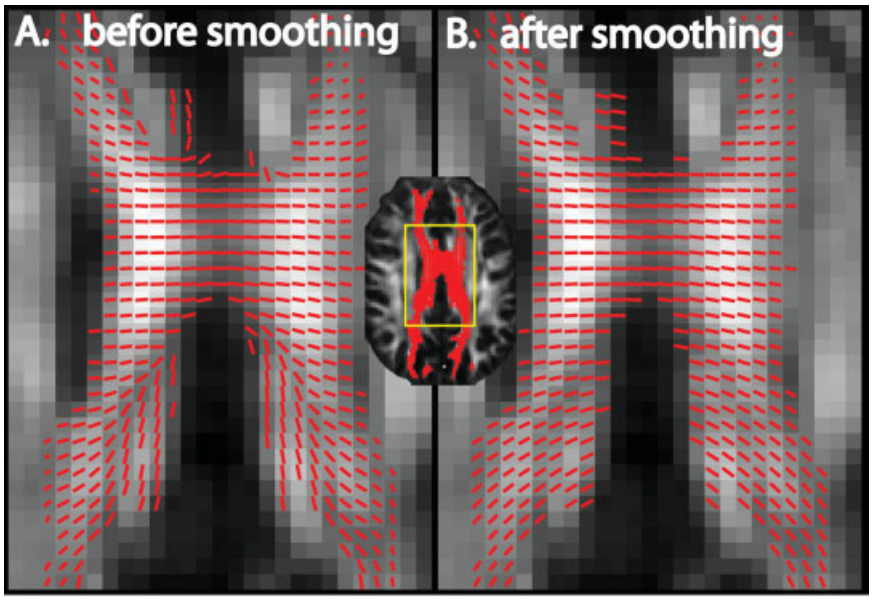

Figure 4.
Fiber orientation smoothing. Diffusion orientations of voxels within manually-selected corpus callosum fiber track ROI are plotted as line segments, overlayed on an axial slice of the FA volume for a control subject (same as in Fig. 3). (**A**) Orientations from diffusion data, before smoothing. (**B**) Orientations after fiber smoothing. [Color figure can be viewed in the online issue, which is available at www.interscience.wiley.com.]

slightly decreased for atlas-derived fiber ROIs. Mean FA was generally lower for atlas-derived fiber ROIs, which could reflect a greater proportion of gray matter in the atlas-derived fiber ROIs [Hua et al., 2008], or could reflect the FA threshold used in the streamline fiber-tracking method. Application of an FA threshold to the atlas-derived fiber ROIs greatly reduced the difference in mean FA between manually selected and atlas-derived fibers, but did not substantially change the results of the group analysis.

Comparison of Control Subjects and Patients With TLE

We used both manually selected fiber tracks and atlas-derived fiber ROIs to compare control subjects and patients with TLE. A general trend common to the results from both methods was that several fibers showed lower FA in patients with left TLE, regardless of hemisphere. This is consistent with some evidence of greater bilateral hippocampal [Bernasconi et al., 2003] and cortical [Bonilha et al., 2007; Keller et al., 2002] pathology in patients with left compared to right TLE. Although the reason for greater brain pathology in left TLE is unclear, it has been proposed that left and right TLE are distinct diseases that have different effects on brain structure [Keller et al., 2002]. Our results suggest that the greater deficits observed in patients with left TLE extend to discrete white matter tracts.

Other Atlas-Based Tractography Methods

Several other methods that are in some sense "atlas-based" have been recently proposed. In 2004, Wakana et al. described what was called a "fiber tract-based atlas"; their atlas was a collection of graphical depictions of manually assisted fiber-tracking results and included a description of methods for reproducibly reconstructing these fiber tracks [Wakana et al., 2004]. More recently, Mori and colleagues used those methods to reconstruct 11 bilateral fiber tracts and created a probabilistic atlas of fiber location [Hua et al., 2008]. Those authors suggested that their atlas-based method would be suitable for an initial screening tool, but might be inferior to the more labor intensive, manually selected fiber tracks. They were concerned about the lower FA in atlas-derived fiber ROIs and suggested that the affine registration method used might be a limiting factor for providing accurate fiber ROIs. They also reported larger between subject coefficients of variation for FA measurements with the atlas-derived fiber ROIs.

An important advance of our method relative to previous methods is the use of fiber orientation information from DI to refine the fiber probability estimates. This individualizes the fiber ROIs for each subject and minimizes the contribution from regions that exhibit diffusion orientations inconsistent with the consensus fiber orientation information contained in the orientation atlas. There are

two other methodological differences that are significant. First, we used nonlinear registration to provide better alignment between subjects and atlas than that provided by affine registration. Second, our image preprocessing included a robust method for B_0 distortion correction, providing excellent registration between diffusion images and the T_1-weighted structural images used to register to atlas space.

Other atlas-based tractography methods generate streamlines from single-subject diffusion images and then use an atlas to label each streamline as belonging to a particular fiber tract. One method for doing so uses a cortical parcellation atlas to select streamline fiber tracks connecting two cortical regions [Lawes et al., 2008; Park et al., 2004; Xia et al., 2005]. Another method is to match single-subject streamlines to an atlas of labeled fiber tracks based on similarity of location and curvature [Maddah et al., 2005; O'Donnell and Westin, 2006, 2007]. A problem common to both approaches is that crossing fibers and noisy diffusion data could degrade performance and lead to stray fibers being included in the resulting fiber tracks. Similarity-based clustering methods using probabilistic fiber-tracking—which is better able to deal with crossing fibers—have been developed [Clayden et al. 2006, 2007]; but stray, artifactual fibers remain a problem. In addition, the large number of iterations required may make whole-brain probabilistic fiber-tracking impractical. In contrast, using our method to generate fiber ROIs for new subjects does not require generating streamlines for each subject. This distinction is particularly important in the case of fiber tracts that happen to be interrupted by a lesion, a situation easily handled by a voxel-wise, probabilistic atlas-based method, but not by streamline fiber-tracking [Hua et al., 2008].

One limitation of selecting fibers based on cortical parcellations, noted by Lawes et al., is that artifactual tracks between unconnected cortical parcels can be generated, requiring careful comparison with known anatomy to distinguish the real from artifactual tracks [Lawes et al., 2008]. Moreover, even though two cortical parcels may in fact have connections, streamlines connecting them may follow alternative, artifactual routes. Thus, some manual editing of fiber tracks for single subjects could be required. Once edited, fiber tracks that accurately model known fiber trajectories between two cortical parcels could be included in a probabilistic atlas such as ours, removing the necessity for future reliance on streamline fiber-tracking in single subjects.

Limitations and Potential Improvements

Our atlas-based fiber identification method shows great promise for use in a variety of research and clinical settings; however, several limitations should be noted. First, our method relies heavily on accurate registration of individual subjects to atlas space using T_1-weighted images. Compared to diffusion weighted images, T_1-weighted images are typically acquired at high resolution (e.g., ~1 mm isotropic) and have high SNR, allowing for robust registration to atlas space. We used the discrete cosine transform (DCT) method for nonlinear registration [Friston et al., 1995], but registration methods with more degrees of freedom, or including DT data [Park et al., 2003], could improve the correspondence of fiber tract locations between subjects. A second potential improvement to our method is to use more parameters to represent the diffusion orientations than the six used by DTs [Frank, 2002; Jansons and Alexander, 2003; Tournier et al., 2004; Tuch, 2004]. Such representations may allow for more accurate estimation of the fractional volume occupied by two or more fibers within a single voxel. Third, our method does not take advantage of information about the relative spatial arrangement of neighboring fiber tracts. Markov random fields could be used to encode the conditional probabilities of neighboring tracts, similar to the method used for the refinement of subcortical segmentations [Fischl et al., 2002]. Finally, the accuracy of the fiber ROIs depends on the quality of the atlas. Stray fibers in the manually selected fiber tracks used to construct the atlas contribute to some degree to the atlas-derived fiber ROIs. This contribution could be reduced or eliminated with substantially more manual editing to trim away the portions of streamlines that stray from the expected route.

Expandability of Fiber Atlas

The fiber atlas we have developed contains most major fiber tracts in the brain. Additional, minor tracts could be added to the atlas, and other tracts, such as corpus callosum, could be further subdivided. Some fiber tracts, such as the optic radiations from LGN to V1 (e.g. Meyer's Loop), were difficult to reconstruct reliably in every subject with the deterministic tracking method we used. Probabilistic fiber-tracking methods, particularly those that explicitly deal with crossing fibers, may be better able to reconstruct these tracts, although manual selection of fiber tracks following the correct path and exclusion of fibers following alternate routes will likely remain necessary. If a known tract can be reliably reconstructed with either probabilistic or deterministic fiber-tracking, it can be added to the probabilistic fiber atlas.

ACKNOWLEDGMENTS

The authors thank Susumu Mori and Hangyi Jiang for providing source code for the FACT fiber tracking program, and Sumiko Abe for creating a 3D fiber track viewer for Linux.

REFERENCES

Basser PJ, Mattiello J, LeBihan D (1994): MR diffusion tensor spectroscopy and imaging. Biophys J 66;259–267.

Basser PJ, Pajevic S, Pierpaoli C, Duda J, Aldroubi A (2000): In vivo fiber tractography using DT-MRI data. Magn Reson Med 44:625–632.

Behrens TE, Woolrich MW, Jenkinson M, Johansen-Berg H, Nunes RG, Clare S, Matthews PM, Brady JM, Smith SM (2003): Characterization and propagation of uncertainty in diffusion-weighted MR imaging. Magn Reson Med 50:1077–1088.

Behrens TE, Berg HJ, Jbabdi S, Rushworth MF, Woolrich MW (2007): Probabilistic diffusion tractography with multiple fibre orientations: What can we gain? Neuroimage 34:144–155.

Berman JI, Berger MS, Chung SW, Nagarajan SS, Henry RG (2007): Accuracy of diffusion tensor magnetic resonance imaging tractography assessed using intraoperative subcortical stimulation mapping and magnetic source imaging. J Neurosurg 107:488–494.

Berman JI, Chung S, Mukherjee P, Hess CP, Han ET, Henry RG (2008): Probabilistic streamline q-ball tractography using the residual bootstrap. Neuroimage 39:215–222.

Bernasconi N, Bernasconi A, Caramanos Z, Antel SB, Andermann F, Arnold DL (2003): Mesial temporal damage in temporal lobe epilepsy: A volumetric MRI study of the hippocampus, amygdala and parahippocampal region. Brain 126(Pt 2):462–469.

Bonilha L, Alessio A, Rorden C, Baylis G, Damasceno BP, Min LL, Cendes F (2007): Extrahippocampal gray matter atrophy and memory impairment in patients with medial temporal lobe epilepsy. Hum Brain Mapp 28:1376–1390.

Catani M, Howard RJ, Pajevic S, Jones DK (2002): Virtual in vivo interactive dissection of white matter fasciculi in the human brain. Neuroimage 17:77–94.

Chang H, Fitzpatrick JM (1992): A technique for accurate magnetic resonance imaging in the presenceof field inhomogeneities. IEEE Trans Med Imaging 11:319–329.

Clayden JD, Bastin ME, Storkey AJ (2006): Improved segmentation reproducibility in group tractography using a quantitative tract similarity measure. Neuroimage 33:482–492.

Clayden JD, Storkey AJ, Bastin ME (2007): A probabilistic model-based approach to consistent white matter tract segmentation. IEEE Trans Med Imaging 26:1555–1561.

Conturo TE, Lori NF, Cull TS, Akbudak E, Snyder AZ, Shimony JS, McKinstry RC, Burton H, Raichle ME (1999): Tracking neuronal fiber pathways in the living human brain. Proc Natl Acad Sci USA 96:10422–10427.

Fischl B, Salat DH, Busa E, Albert M, Dieterich M, Haselgrove C, van der Kouwe A, Killiany R, Kennedy D, Klaveness S, Montillo A, Makris N, Rosen B, Dale AM (2002): Whole brain segmentation: Automated labeling of neuroanatomical structures in the human brain. Neuron 33:341–355.

Frank LR (2002): Characterization of anisotropy in high angular resolution diffusion-weighted MRI. Magn Reson Med 47:1083–1099.

Friman O, Farneback G, Westin CF (2006): A Bayesian approach for stochastic white matter tractography. IEEE Trans Med Imaging 25:965–978.

Friston KJ, Ashburner J, Frith CD, Poline J-B, Heather JD, Frackowiak RSJ (1995): Spatial registration and normalization of images. Hum Brain Mapp 3:165–189.

Genovese CR, Lazar NA, Nichols T (2002): Thresholding of statistical maps in functional neuroimaging using the false discovery rate. Neuroimage 15:870–878.

Hua K, Zhang J, Wakana S, Jiang H, Li X, Reich DS, Calabresi PA, Pekar JJ, van Zijl PC, Mori S (2008): Tract probability maps in stereotaxic spaces: Analyses of white matter anatomy and tract-specific quantification. Neuroimage 39:336–347.

Jansons KM, Alexander DC (2003): Persistent angular structure: New insights from diffusion MRI data. Dummy version. Inf Process Med Imaging 18:672–683.

Jones DK, Pierpaoli C (2005): Confidence mapping in diffusion tensor magnetic resonance imaging tractography using a bootstrap approach. Magn Reson Med 53:1143–1149.

Jovicich J, Czanner S, Greve D, Haley E, van der Kouwe A, Gollub R, Kennedy D, Schmitt F, Brown G, Macfall J, Fischl B, Dale A (2006): Reliability in multi-site structural MRI studies: Effects of gradient non-linearity correction on phantom and human data. Neuroimage 30:436–443.

Keller SS, Mackay CE, Barrick TR, Wieshmann UC, Howard MA, Roberts N (2002): Voxel-based morphometric comparison of hippocampal and extrahippocampal abnormalities in patients with left and right hippocampal atrophy. Neuroimage 16:23–31.

Lawes IN, Barrick TR, Murugam V, Spierings N, Evans DR, Song M, Clark CA (2008): Atlas-based segmentation of white matter tracts of the human brain using diffusion tensor tractography and comparison with classical dissection. Neuroimage 39:62–79.

Lazar M, Alexander AL (2005): Bootstrap white matter tractography (BOOT-TRAC). Neuroimage 24:524–532.

Leventon ME, Grimson WE (1998): Multi-modal volume registration using joint intensity distributions. Med Image Comput Comput Assist Interv 1496:1057–1066.

Maddah M, Mewes AU, Haker S, Grimson WE, Warfield SK (2005): Automated atlas-based clustering of white matter fiber tracts from DTMRI. Med Image Comput Comput Assist Interv Int Conf Med Image Comput Comput Assist Interv 8(Pt 1):188–195.

Morgan PS, Bowtell RW, McIntyre DJ, Worthington BS (2004): Correction of spatial distortion in EPI due to inhomogeneous static magnetic fields using the reversed gradient method. J Magn Reson Imaging 19:499–507.

Mori S, Crain BJ, Chacko VP, van Zijl PC (1999): Three-dimensional tracking of axonal projections in the brain by magnetic resonance imaging. Ann Neurol 45:265–269.

Mori S, Kaufmann WE, Davatzikos C, Stieltjes B, Amodei L, Fredericksen K, Pearlson GD, Melhem ER, Solaiyappan M, Raymond GV, Moser HW, van Zijl PC (2002): Imaging cortical association tracts in the human brain using diffusion-tensor-based axonal tracking. Magn Reson Med 47:215–223.

O'Donnell L, Westin CF (2006): High-dimensional white matter atlas generation and group analysis. Med Image Comput Comput Assist Interv Int Conf Med Image Comput Comput Assist Interv 9(Pt 2):243–251.

O'Donnell LJ, Westin CF (2007): Automatic tractography segmentation using a high-dimensional white matter atlas. IEEE Trans Med Imaging 26:1562–1575.

Oldfield RC (1971): The assessment and analysis of handedness: The Edinburgh inventory. Neuropsychologia 9:97–113.

Park HJ, Kubicki M, Shenton ME, Guimond A, McCarley RW, Maier SE, Kikinis R, Jolesz FA, Westin CF (2003): Spatial normalization of diffusion tensor MRI using multiple channels. Neuroimage 20:1995–2009.

Park HJ, Kubicki M, Westin CF, Talos IF, Brun A, Peiper S, Kikinis R, Jolesz FA, McCarley RW, Shenton ME (2004): Method for combining information from white matter fiber tracking and gray matter parcellation. AJNR Am J Neuroradiol 25:1318–1324.

Parker GJ, Stephan KE, Barker GJ, Rowe JB, MacManus DG, Wheeler-Kingshott CA, Ciccarelli O, Passingham RE, Spinks RL, Lemon RN, Turner R (2002): Initial demonstration of in vivo tracing of axonal projections in the macaque brain and comparison with the human brain using diffusion tensor imaging and fast marching tractography. Neuroimage 15:797–809.

Poupon C, Clark CA, Frouin V, Regis J, Bloch I, Le Bihan D, Mangin J (2000): Regularization of diffusion-based direction maps for the tracking of brain white matter fascicles. Neuroimage 12:184–195.

Reinsberg SA, Doran SJ, Charles-Edwards EM, Leach MO (2005): A complete distortion correction for MR images: II. Rectification of static-field inhomogeneities by similarity-based profile mapping. Phys Med Biol 50:2651–2661.

Stieltjes B, Kaufmann WE, van Zijl PC, Fredericksen K, Pearlson GD, Solaiyappan M, Mori S (2001): Diffusion tensor imaging and axonal tracking in the human brainstem. Neuroimage 14:723–735.

Tournier JD, Calamante F, Gadian DG, Connelly A (2004): Direct estimation of the fiber orientation density function from diffusion-weighted MRI data using spherical deconvolution. Neuroimage 23:1176–1185.

Tuch DS (2004): Q-ball imaging. Magn Reson Med 52:1358–1372.

Wakana S, Caprihan A, Panzenboeck MM, Fallon JH, Perry M, Gollub RL, Hua K, Zhang J, Jiang H, Dubey P, Blitz A, van Zijl P, Mori S (2007): Reproducibility of quantitative tractography methods applied to cerebral white matter. Neuroimage 36:630–644.

Wakana S, Jiang H, Nagae-Poetscher LM, van Zijl PC, Mori S (2004): Fiber tract-based atlas of human white matter anatomy. Radiology 230:77–87.

Xia Y, Turken U, Whitfield-Gabrieli SL, Gabrieli JD (2005): Knowledge-based classification of neuronal fibers in entire brain. Med Image Comput Comput Assist Interv Int Conf Med Image Comput Comput Assist Interv 8(Pt 1):205–212.

Yogarajah M, Duncan JS (2007): Diffusion-based magnetic resonance imaging and tractography in epilepsy. Epilepsia 49:189–200.